Earth and Planetary Science Letters 303 (2011) 37–47

Contents lists available at ScienceDirect

Earth and Planetary Science Letters

journal homepage: www.elsevier.com/locate/epsl

Assimilation of the plutonic roots of the Andean arc controls variations in U-series disequilibria at Volcan Llaima, Chile

O. Reubi [a,b,*], B. Bourdon [a,1], M.A. Dungan [b], J.M. Koornneef [a], D. Sellés [c,d], C.H. Langmuir [c], S. Aciego [a]

[a] ETH Zurich, Institute of Geochemistry and Petrology, Switzerland
[b] University of Geneva, Earth Sciences, Switzerland
[c] Harvard University, Earth and Planetary Sciences, USA
[d] Sernageomin, Chile

ARTICLE INFO

Article history:
Received 12 October 2010
Received in revised form 6 December 2010
Accepted 7 December 2010
Available online 21 January 2011

Editor: T.M. Harrison

Keywords:
U-series
assimilation
arc magmatism
basaltic andesite

ABSTRACT

U-series disequilibria provide important constraints on the processes and time scales of melt production, differentiation, and transport in subduction settings. Such constraints, which are essential for understanding the chemical evolution of the continental crust, are conventionally based on the assumption that the U-series disequilibria measured in mafic lavas are produced during mantle metasomatism and melting, and that intracrustal differentiation and assimilation have limited impacts. Here we show that mantle-derived U-series disequilibria in mafic lavas erupted at Volcán Llaima, Chile are significantly diminished by assimilation of plutonic rocks forming Llaima's subvolcanic basement. This contamination process is extremely subtle in terms of "classical" indicators of crustal assimilation like Sr, Nd or Pb isotopes because it is a manifestation of assimilative recycling of the plutonic roots of the arc. This process results in variations in U-series disequilibria and incompatible trace element ratios that are significant compared to regional and global variability in arc magmas. Furthermore, it yields linear correlations between U-series excesses and incompatible trace element ratios that are generally interpreted as slab-fluid indicators and chronometers, or tracers of sediment recycling in subduction zone. Cannibalization of ancestral magmas by ascending melts warrants careful evaluation when considering the components and chemical fluxes in subduction zones. Linear arrays defined by activity ratios of U-series nuclides with different half-lives may be the most reliable indicators of assimilative recycling of ancestral intrusive magmas.

1. Introduction

Disequilibria between short-lived nuclides produced in radioactive decay chains of U and Th are excellent time-dependent tracers of magmatic processes. U-series disequilibria measured in arc magmas can provide constraints on the processes and time scales of mantle metasomatism, melt production, magma differentiation, and mass transport above subduction zones (see, Turner et al., 2003, and references herein). These constraints are essential for quantifying chemical fluxes through subduction zones, with important implications for the chemical evolution of the continental crust, the dynamics volcanic eruptions, and the formation of ore deposits.

Arc lavas generally have excesses of ^{238}U over ^{230}Th [i.e. ($^{230}Th/^{238}U$)<1; where parentheses denote activity ratios] and large excesses of ^{226}Ra relative to ^{230}Th. As both U and Ra are fluid mobile elements, and these excesses correlate with trace element ratios indicative of metasomatism by fluids (e.g. Ba/Th), they are generally attributed to recent addition of slab-fluid to the mantle wedge (Allegre and Condomines, 1982; Elliott et al., 1997; Gill and Williams, 1990; McDermott and Hawkesworth, 1991; Turner and Hawkesworth, 1997; Turner et al., 2000). The broad linear correlations between ($^{230}Th/^{232}Th$) and ($^{238}U/^{232}Th$) observed for suites of lavas from single arc have been interpreted as an indication that the time span between fluid addition to the mantle wedge and eruption is typically between 20 and 150 kyr (Sigmarsson et al., 1990; Turner and Hawkesworth, 1997; Turner et al., 2001). Preservation of ^{226}Ra excesses in arc magmas indicate much shorter time scales, possibly as short as few hundred years (Turner et al., 2001). These apparent discrepancies in the time scales of slab fluid addition have been interpreted to result from multistage dehydration events in which the first fluid fluxes contain ^{238}U and ^{226}Ra, when the last fluids expelled contain only ^{226}Ra produce by in-growth from residual ^{230}Th in the slab (Turner et al., 2000). The excesses of ^{231}Pa over ^{235}U observed in the majority of arc lavas are taken as an indication that the effects of partial melting processes overprint those of slab-fluid (Bourdon et al., 1999; Huang and Lundstrom, 2007; Pickett and Murrell, 1997; Thomas et al., 2002; Turner et al., 2006). The broad negative correlation between average ($^{231}Pa/^{235}U$) and convergence rate in all arc settings has been

* Corresponding author.
E-mail address: olivier.reubi@erdw.ethz.ch (O. Reubi).
[1] Now at: Ecole Normale Supérieure de Lyon and CNRS, France.

0012-821X/$ – see front matter © 2010 Elsevier B.V. All rights reserved.
doi:10.1016/j.epsl.2010.12.018

interpreted as an indication that mantle melting rates strongly control ^{231}Pa excesses and are coupled to the subduction rate (Huang and Lundstrom, 2007; Turner et al., 2006).

These constraints on the time scales and processes of mantle metasomatism and partial melting are obtained from regional to global data sets. However, detailed studies on single volcanoes often reveal significant ranges in U-series disequilibria with respect to regional and global variations (e.g. Turner et al., 2007; Yokoyama et al., 2006), demonstrating that second-order local processes operating over relatively short time scales may modify mantle-derived U-series disequilibria. Several recent studies have shown that processes affecting the magmas during ascent through the crust (e.g. crustal assimilation, crystallization) can have significant leverage on U-series disequilibria (e.g. Bourdon et al., 2000; Garrison et al., 2006; Handley et al., 2008; Huang et al., 2008; Price et al., 2007; Yokoyama et al., 2006). To which extent crustal processes may have modified the signature of primary genetic processes (e.g. fluid addition to the mantle wedge, partial melting regime) needs to be considered to ascertain the reliability of time scales inferred from regional to global U-series data sets.

Here, we investigate the extent and cause of local and short-term temporal variability in U-series disequilibria in lavas from Volcán Llaima, Chile, one of the most historically active volcanoes in South America. To this end, we measured isotope concentrations of U, Pa, Th and Ra by mass spectrometry on multiple samples from each historic eruptive event for which vents and timing are reasonably well documented (Naranjo and Moreno, 2005).

2. Geological setting

Volcán Llaima, Chile is one of the most historically active volcanoes in South America. It is located at 38.7 °S in the Andean Southern Volcanic Zone (SVZ; 33–46 °S) (Fig. 1). The SVZ overlay the section of the subducting slab bounded to the north and south respectively by the subducted Juan Fernandez Ridge and the Chile Rise. The Nazca oceanic plate being subducted beneath the central SVZ is ~30 Ma old and converges on the Andean margin at a rate of ~10 cm/yr (Tassara et al., 2007). The SVZ segment in which Llaima is located is underlain by 30–40 km thick continental crust and is characterized by the predominance of basaltic andesite stratovolcanoes whose magmas show relatively minor elemental or isotopic (Nd–Sr–Pb–O) indications of crustal contamination on their magma chemistry (Hickey et al., 1986; Hickey-Vargas et al., 2002; Tormey et al., 1991). The Andean crust thickens to 55 km from 36 to 33 °S and andesite to dacite magmas with geochemical features indicative of significant crustal contamination predominate (Davidson et al., 1988; Hickey et al., 1986; Hildreth and Moorbath, 1988). The subvolcanic basement beneath Llaima comprises Tertiary diorite to granodiorite plutons related to earlier magmatism of the arc (Lucassen et al., 2004) (Fig. 1).

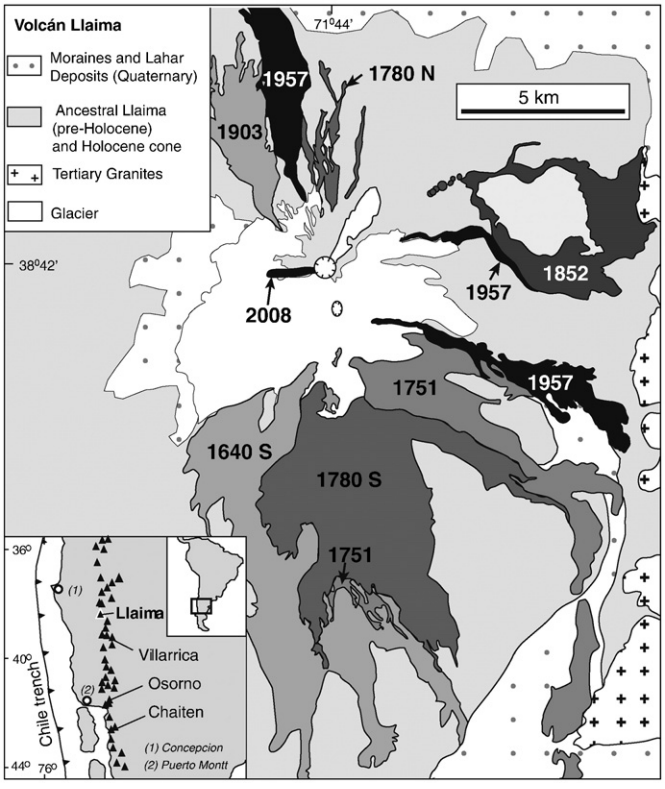

Fig. 1. Geological map of Volcán Llaima modified from Naranjo and Moreno (2005). The map focuses on the Holocene cone. Historic lava flows are represented by grey shaded areas labeled with the eruption year. Note the Tertiary granites that outcrop on the eastern side of Volcán Llaima. Inset map shows that location of Volcán Llaima in the Andean Southern Volcanic Zone.

Holocene volcanic activity at Llaima began with caldera collapse and eruption of the basaltic to andesitic (~52–58% SiO_2, our unpublished data) Curacautin Ignimbrite (~13.5 ka). Eruptions from a N–S central-vent system and oblique-trending flank fissures buried this caldera during the late Holocene. Historical volcanic activity of Llaima consists predominantly of Strombolian events. Six major effusive eruptions occurred between 1640 and 1957 (Fig. 1). The most recent eruptive activity started in May 2007 and it has been marked by short but vigorous Strombolian phases in January 2008 and April 2009, both of which subsequently produced small lava flows. Samples representative of the historical activity are presented here and were selected from a sample collection that includes more than 450 samples analyzed for major elements by XRF (Dungan et al., unpublished results). All historical samples are evolved basalts (>51% SiO_2, <6.5% MgO) to basaltic andesites (<55% SiO_2, >3.9% MgO) and contain mineral assemblages with widely variable proportions of plagioclase, olivine, one or two pyroxenes, and spinel.

3. Analytical techniques

Major elements were determined by X-ray fluorescence (XRF) on fused glass discs on a Phillips PW 2400 spectrometer equipped with a rhodium tube at the University of Lausanne (Switzerland), following the methods described by Pfeifer et al. (1991). Trace element concentrations were determined using a Thermo X-series ICP-MS quadrupole at Harvard University. The samples (50 mg) were processed using the method described in Bezos et al. (2009). ^{72}Ge, ^{103}Rh, ^{115}In, ^{169}Tm, and ^{209}Bi were used for internal standard normalization and the following rocks were used for calibration curves: BHVO-2, BCR-2, AGV-1, DNC-1, and JB-2, as well as the in-house standard Mid-Atlantic Ridge basalt (MAR). The in-house standard K1919 was also analyzed and used for drift correction. Trace element data obtained by ICP-MS are accurate to within ± 5% on the basis of duplicate analyses.

Neodymium isotopic ratios were measured on a Nu Instrument® MC-ICP-MS at ETH Zurich. For each sample, about 100 mg of rock powder was digested in a mixture of HF–HNO_3, followed by neodymium separation by extraction chromatography using Eichrom TRU and LN spec resins columns following the procedure of Pin and Zalduegui (1997). The sample solutions were introduced using an Apex desolvation system. ^{143}Nd/^{144}Nd isotope ratios were corrected for mass fractionation using a ^{146}Nd/^{144}Nd ratio of 0.7219 and normalized to the JNdi-1 standard value of 0.512115 (Tanaka et al., 2000). Repeated measurements of JNdi-1 during the analysis period yielded a mean ^{143}Nd/^{144}Nd = 0.512111 ± 29 (2 S.D. n = 14).

Full details of the chemical separation and analytical techniques used for U-series analyses are given in Koornneef et al. (2010), and an outline is given here. U, Pa, Th, and Ra concentrations and isotope ratios were determined on single aliquots (about 800 mg) spiked with ^{236}U, ^{229}Th, ^{233} Pa, and ^{228}Ra tracers before dissolution in HF–HNO_3

mixture. U, Pa, Th, and Ra purification was achieved using a combination of EiChrom® TRU-spec and Sr-spec, and Bio-Rad® AG 1-X4, AG 1-X8 and AG50W-X8 resin columns. Concentrations and isotope ratios were measured on a Nu Instrument® MC-ICP-MS at ETH Zurich. Analyses of rock standard in secular equilibrium performed concurrently with the samples yielded the following results: U = 1.691 ± 0.003 ppm, Th = 5.87 ± 0.04 ppm, ($^{234}U/^{238}U$) = 1.002 ± 0.004, ($^{231}Pa/^{235}U$) = 1.012 ± 0.022; ($^{230}Th/^{238}U$) = 0.998 ± 0.011, ($^{230}Th/^{232}Th$) = 0.875 ± 0.021, ($^{226}Ra/^{230}Th$) = 1.008 ± 0.024 for BCR-2; and U = 0.502 ± 0.006 ppm, Th = 2.127 ± 0.021 ppm, ($^{234}U/^{238}U$) = 1.004 ± 0.008, ($^{231}Pa/^{235}U$) = 0.999 ± 0.016, ($^{230}Th/^{238}U$) = 0.996 ± 0.014, ($^{230}Th/^{232}Th$) = 0.714 ± 0.009, and ($^{226}Ra/^{230}Th$) = 1.007 ± 0.030 for W2.

4. Results

4.1. Major and trace elements

Llaima historical magmas show major element trends with decreasing MgO, CaO, Fe_2O_3 and Al_2O_3, and increasing K_2O and TiO_2, while SiO_2 content increases (Fig. 2 and Table 1). The ranges of major elements contents observed at a given SiO_2 content indicate that these magmas do not follow a simple liquid line of descent. Either distinct fractionation paths or open system processes, such as magma mixing and crustal assimilation are required. Alkali elements show a moderate increase during differentiation suggesting a limited role of crustal assimilation compared to others SVZ volcanoes (Fig. 2b).

Llaima magmas have typical subduction-related trace element signatures. Large ion lithophile elements (LILE) are enriched relative to LREE (Ba/La 23.3–27.4) and both are enriched relative to high field strength elements (HFSE) (Ba/Nb 75.5–99.2; La/Nb 3.0–3.6). Llaima lavas have trace element contents similar to others SVZ magmas but show limited ranges in HFSE contents and La/Sm ratios compared the SVZ ranges (Fig. 2c and d). HFSE abundances are moderately enriched relative to N-MORB values: e.g. Nb/Yb = 1.0–1.2, compared with 0.8 for average N-MORB (Sun and McDonough, 1989).

4.2. Neodymium isotopes

New $^{143}Nd/^{144}Nd$ isotopic compositions of Llaima lavas define a limited range from 0.512878 to 0.512899 that encompass previously published values (Hickey et al., 1986) (Table 1). Llaima lavas have among the highest Nd isotope ratios in the SVZ, a general feature of volcanoes of the central and southern SVZ (38–41°S) (Hickey et al., 1986; Hildreth and Moorbath, 1988). No correlation is observed between Nd isotope ratios and incompatible element abundances or ratios. Tertiary granites located near Llaima have $^{143}Nd/^{144}Nd$ isotopic compositions (0.512850–512858) similar to Llaima magmas, and are distinctly higher than sediments (0.512673–0.512787) currently entering the subduction zone at these latitudes (Lucassen et al., 2009).

4.3. Uranium series isotopes

Llaima lavas are characterized by ^{238}U, ^{231}Pa, and ^{226}Ra excesses typical of arc magmas (Figs. 3 and 4) (see Turner et al., 2003, and

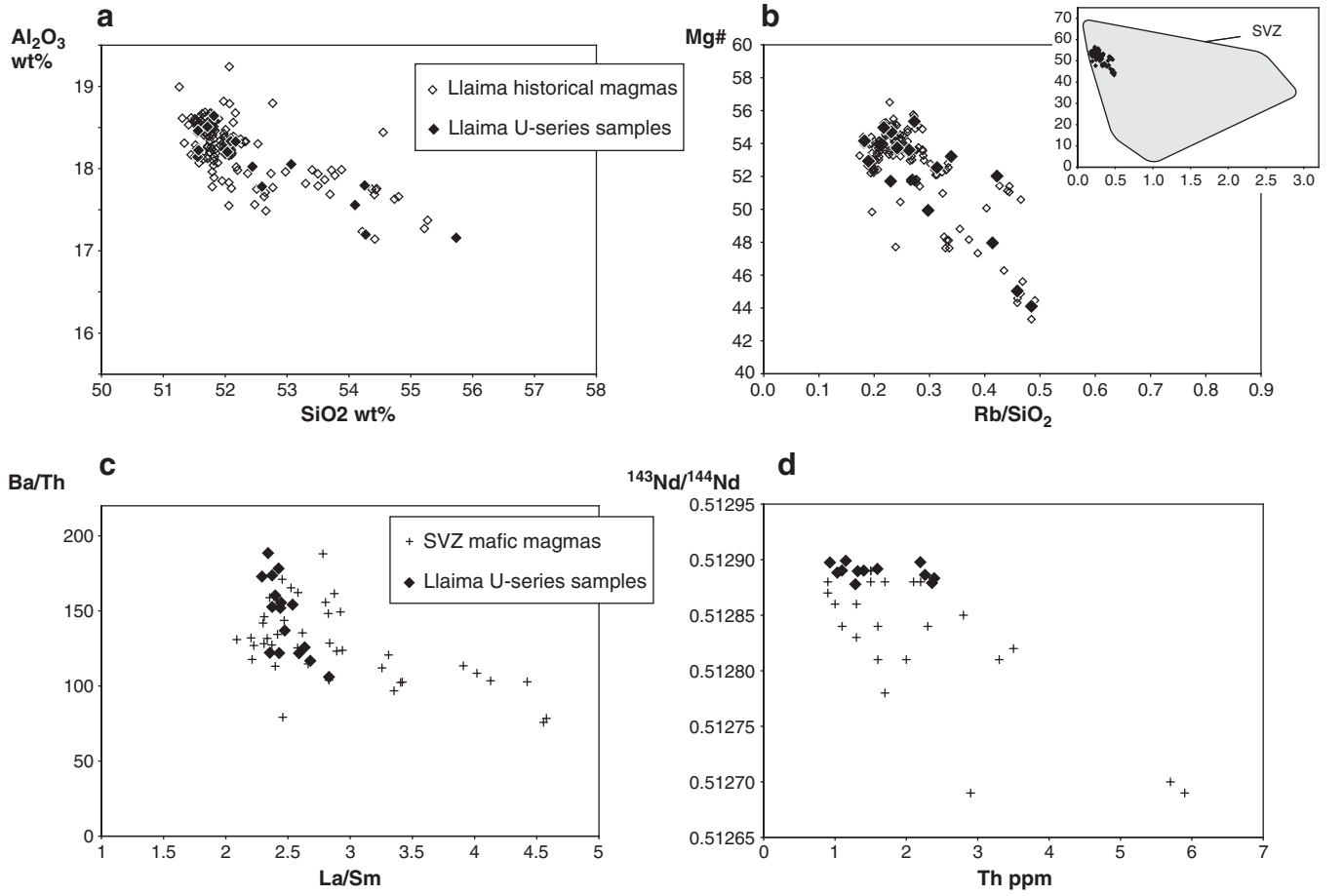

Fig. 2. Major and trace elements and Nd isotope variation diagrams for Llaima historical (1640 to 2009) lavas and the Andean Southern Volcanic Zone (SVZ) mafic magmas. (a) Al_2O_3 vs. SiO_2. (b) Mg# vs. Rb/SiO_2. (C) Ba/Th vs. La/Sm. (d) $^{143}Nd/^{144}Nd$ isotopes vs. Th. Black diamonds are Llaima samples measured for U-series and reported in Table 1, open diamonds are all Llaima historical magmas measured for major elements (Dungan, unpublished data). Crosses in (c) and (d) are SVZ data from Hickey et al. (1986).

Table 1
Major (wt.%) and trace (ppm) concentrations, and Nd isotope compositions for Volcán Llaima lavas.

Eruption	2008	1957	1957	1780 SSW	1780 N	1780 SE	1780 S	1751	1903 S	1640	1640 S	1640 S	1903	1852	1852	1852
Sample	508	12c	61	33	89	19	208	7	95	31	385	252	85	76	74c	23
SiO_2	52.0	52.1	51.7	52.1	52.6	51.6	51.6	51.6	54.3	54.3	55.7	52.2	53.1	52.4	54.1	51.8
TiO_2	1.11	1.02	1.04	0.95	1.10	1.01	1.04	1.03	0.98	1.31	1.22	1.01	1.00	1.18	1.15	1.06
Al_2O_3	17.7	17.8	18.0	17.8	17.3	17.7	18.0	17.6	17.3	16.7	16.7	17.8	17.6	17.5	17.1	18.1
Fe_2O_3	10.2	9.8	9.8	9.6	10.1	10.0	10.0	10.1	9.2	10.3	9.8	9.9	9.6	10.3	9.8	9.9
MnO	0.16	0.16	0.16	0.16	0.16	0.16	0.16	0.16	0.15	0.17	0.17	0.16	0.16	0.17	0.16	0.16
MgO	5.54	5.69	5.59	5.99	5.63	6.16	5.94	6.15	5.05	4.27	3.91	5.80	5.49	5.16	4.54	5.34
CaO	9.53	9.52	9.82	9.57	9.03	9.66	9.54	9.57	8.80	8.18	7.81	9.52	9.17	9.11	8.75	9.65
Na_2O	2.82	3.06	3.06	3.03	3.12	2.98	2.87	3.03	3.18	3.48	3.37	2.83	3.09	3.20	3.34	3.15
K_2O	0.69	0.66	0.59	0.63	0.81	0.57	0.54	0.59	0.90	1.03	1.07	0.61	0.75	0.74	0.91	0.61
P_2O_5	0.20	0.19	0.18	0.16	0.21	0.18	0.18	0.18	0.17	0.26	0.24	0.17	0.18	0.22	0.23	0.18
Total	100	100	100	100	100	100	100	100	100	100	100	100	100	100	100	100
Li	10.5	9.69	8.25	9.27	10.4	8.35	9.19	9.58	10.4	13.24	13.1	8.49	9.30	10.6	11.6	8.65
Be	0.993	0.895	0.803	0.881	1.01	0.848	0.886	0.823	0.949	1.23	1.29	0.899	0.895	0.952	1.07	0.909
B		15.6	10.4	12.4	15.3	15.6		13.9	11.8	21.2			13.3	17.2	17.7	13.9
P	0.213	0.193	0.189	0.168	0.211	0.182	0.181	0.192	0.179	0.269	0.248	0.177	0.183	0.228	0.242	0.194
Sc	31.5	28.8	25.3	24.4	25.9	29.0	28.8	30.7	20.4	26.7	23.9	31.5	24.8	23.2	31.5	24.3
V	252	239	270	232	251	243	241	246	234	259	244	237	241	261	254	248
Cr	80.9	81.6	93.3	94.9	79.0	94.6	79.0	98.9	67.9	44.8	37.6	79.0	83.7	55.0	63.3	79.3
Mn	0.166	0.152	0.154	0.150	0.157	0.155	0.163	0.158	0.148	0.160	0.165	0.162	0.152	0.160	0.154	0.156
Co	33.0	32.4	31.8	32.9	32.8	34.5	34.1	34.7	29.2	27.9	25.8	33.6	31.4	31.1	27.6	31.5
Ni	45.2	45.6	41.5	53.5	49.7	55.1	50.9	55.6	38.0	27.7	21.7	48.3	45.2	38.8	23.9	41.4
Cu	120	106	98	100	114	108	105	110	98	127	96	102	102	123	115	112
Zn	86.6	79.8	80.4	76.2	85.1	81.1	84.5	83.3	76.9	93.9	93.1	83.1	79.1	88.4	85.7	83.8
Ga	18.4	17.8	17.9	17.4	18.1	17.6	18.5	17.9	17.4	18.2	18.8	17.9	17.8	18.4	18.1	18.3
Rb	14.7	14.7	10.8	14.0	17.7	12.1	10.4	13.1	24.7	24.2	26.6	13.1	18.8	16.6	23.8	12.4
Sr	453	475	488	468	482	456	476	455	475	412	403	440	494	451	441	494
Y	23.4	20.9	20.6	19.5	24.6	21.1	20.1	22.4	21.8	32.0	28.6	21.1	21.7	25.3	26.0	22.1
Zr	88.9	80.2	75.8	73.1	93.2	76.2	73.9	78.8	88.6	131.2	120.9	75.6	83.4	98.7	106.3	81.6
Nb	2.57	2.48	2.30	2.15	2.64	2.17	2.18	2.29	2.55	3.53	3.23	2.07	2.38	2.89	3.12	2.35
Mo	0.791	0.557	0.799	0.476	0.591	0.530	0.564	0.581	0.498	0.925	0.914	0.522	0.504	0.685	0.904	0.597
Sn	0.874	0.866	0.830	0.741	1.009	0.852	0.727	0.847	1.11	1.33	1.06	0.728	0.863	1.04	0.993	0.913
Cs	1.15	1.01	0.411	0.891	1.17	0.951	0.858	0.981	1.12	1.82	1.70	0.977	1.03	1.24	1.33	0.981
Ba	200	198	184	194	223	177	175	185	253	268	287	180	222	218	264	189
La	8.46	8.18	7.75	7.09	9.07	7.36	7.04	7.74	9.32	10.8	11.0	7.15	8.52	9.36	10.8	7.54
Ce	20.4	19.2	18.2	17.6	21.6	17.5	17.1	18.2	21.4	27.7	26.5	17.2	20.0	22.1	25.0	18.7
Pr	2.95	2.71	2.56	2.34	3.07	2.52	2.52	2.58	2.91	3.72	3.70	2.51	2.78	3.10	3.47	2.62
Nd	13.8	12.7	12.3	11.5	14.2	12.0	11.7	12.4	13.2	17.6	17.0	11.7	12.8	14.8	15.9	12.6
Sm	3.47	3.22	3.20	2.92	3.66	3.10	3.01	3.23	3.29	4.58	4.26	3.01	3.24	3.83	4.01	3.29
Eu	1.10	1.03	1.06	0.99	1.14	1.02	1.02	1.05	1.05	1.31	1.25	1.01	1.05	1.17	1.21	1.08
Gd	4.01	3.55	3.55	3.30	4.02	3.52	3.50	3.66	3.60	5.19	4.90	3.53	3.57	4.27	4.40	3.68
Tb	0.640	0.576	0.573	0.527	0.657	0.567	0.550	0.593	0.593	0.848	0.784	0.566	0.586	0.691	0.705	0.604
Dy	3.93	3.53	3.50	3.24	3.99	3.51	3.40	3.67	3.62	5.28	4.85	3.51	3.56	4.26	4.28	3.70
Ho	0.824	0.734	0.724	0.678	0.833	0.732	0.711	0.758	0.749	1.11	1.02	0.742	0.736	0.879	0.886	0.776
Er	2.34	2.10	2.08	1.94	2.40	2.10	2.02	2.18	2.15	3.18	2.92	2.10	2.14	2.53	2.56	2.23
Yb	2.28	2.08	2.05	1.90	2.39	2.08	1.97	2.15	2.17	3.15	2.88	2.08	2.13	2.49	2.55	2.19
Lu	0.362	0.325	0.317	0.299	0.368	0.327	0.314	0.336	0.336	0.501	0.457	0.327	0.334	0.386	0.397	0.341
Hf	2.35	2.14	2.01	1.96	2.48	2.03	1.96	2.11	2.38	3.41	3.22	2.03	2.23	2.61	2.77	2.17
Ta	0.151	0.144	0.132	0.130	0.158	0.124	0.127	0.132	0.164	0.207	0.197	0.125	0.148	0.168	0.193	0.138
W	0.184	0.259	0.201	0.202	0.246	0.225	0.192	0.231	0.193	0.360	0.599	0.188	0.211	0.282	0.319	0.181
Tl	0.061	0.079	0.053	0.082	0.104	0.072	0.055	0.072	0.109	0.149	0.127	0.062	0.103	0.099	0.131	0.087
Pb	7.75	8.33	7.73	7.56	9.58	6.59	5.35	7.20	7.89	12.62	8.71	6.10	8.87	9.47	9.27	7.79
Th	1.32	1.29	1.03	1.59	1.63	1.02	0.93	1.15	2.39	2.19	2.36	1.18	1.77	1.40	2.26	1.10
U	0.482	0.460	0.388	0.466	0.551	0.379	0.352	0.408	0.720	0.764	0.806	0.423	0.573	0.524	0.702	0.402
$^{143}Nd/^{144}Nd$	0.512890	0.512878	0.512888	0.512892			0.512897	0.512899	0.512883	0.512898	0.512879			0.512890	0.512886	0.512890
2σm	±7	±7	±7	±9			±7	±6	±8	±7	±6			±6	±8	±9

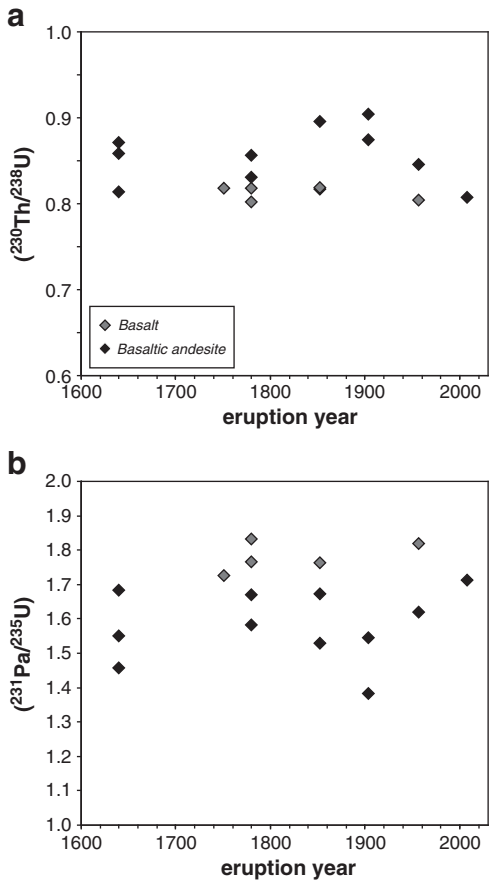

Fig. 3. Temporal variations in (^{230}Th/^{238}U) and (^{231}Pa/^{235}U) disequilibria of historical lavas from Llaima. The variability in U-series disequilibria observed at the scale of a single eruption suggest that upper crustal processes rather than mantle processes controlled the U-series disequilibria. Error bars are smaller than symbol size.

references herein). Significant variations in U-series disequilibria and incompatible element ratios are observed among multiple samples from single eruptive events (Fig. 3). (^{231}Pa/^{235}U) ratios in the 1640 lavas range from 1.38 to 1.68, representing 66% of the total range. Key features of the Llaima data set (Table 2) are strong correlations between ^{238}U and ^{231}Pa excesses and LILE/HFSE and LREE/HFSE ratios (Fig. 4). (^{231}Pa/^{235}U) activity ratios correlate positively with Ba/Th and Ce/Th, and negatively with Rb/Zr and Th/La. Opposite correlations are observed between (^{230}Th/^{238}U) and these ratios. (^{226}Ra/^{230}Th) ratios show no correlation with ^{238}U excesses or LILE/HFSE ratios (Fig. 5a). On the U–Th equiline diagram, Llaima magmas form an inclined linear array, wherein lavas with the greatest ^{238}U excesses and U/Th ratios also have the highest (^{230}Th/^{232}Th) ratios (Fig. 4c). For all samples, (^{234}U/^{238}U) activity ratios are within error of equilibrium, indicating that the samples have not suffered secondary alteration. Llaima magmas fall on the slab fluid contribution end (i.e. highest ^{238}U and ^{226}Ra excesses) of the regional trend defined by Sigmarsson et al. (2002), but the ranges defined by Llaima data encompass a large fraction of the regional variability (Fig. 4c). The variability in U-series disequilibria observed at the scale of a single eruption, and the clear correlation between U-series activity ratios and trace element ratios, are important observations for the following discussion.

5. Discussion

5.1. Controls on U–Th and U–Pa arrays

The linear array between (^{231}Pa/^{235}U) and (^{230}Th/^{238}U) pointing toward secular equilibrium (Fig. 4a) is a remarkable feature of Llaima historical magmas and needs to be accounted for in geochemical models. ^{231}Pa excesses in arc lavas are considered to be generated by partial melting in the mantle wedge (Bourdon et al., 1999; Pickett and Murrell, 1997; Thomas et al., 2002; Turner et al., 2006), whilst ^{238}U excesses are thought to result from U addition to the mantle wedge by slab fluids (Allegre and Condomines, 1982; Gill and Williams, 1990; Sigmarsson et al., 1990). Coupling between slab fluid flux and partial melting dynamics may produce correlated (^{231}Pa/^{235}U) and (^{230}Th/^{238}U). Fluid flux melting models predict that (^{231}Pa/^{235}U) and (^{230}Th/^{238}U) ratios should be correlated and should both diminish with increasing enrichment in large ion lithophile elements relative to high field strength elements (e.g. Ba/Th) produced by slab-fluid addition (Dosseto et al., 2003; Thomas et al., 2002). A strong positive correlation between (^{231}Pa/^{235}U) and Ba/Th (Fig. 4b) is observed at Llaima. This precludes coupled fluid flux and partial melting as the mechanism controlling these linear arrays. In addition, the linearity of these arrays eliminates variable ageing of magmas between production in the mantle and eruption as the controlling process. Llaima magmas are relatively differentiated basaltic andesites with MgO <6.5 wt.%, implying significant fractional crystallization from primary magmas in equilibrium with mantle peridotite. U, Th, and Pa are all strongly incompatible with respect to the mineral assemblage olivine, pyroxenes, and plagioclase (Blundy and Wood, 2003), and fractional crystallization cannot change element ratios sufficiently to produce the observed range in U–Th and U–Pa disequilibria. We conclude that the correlations among Pa–U–Th disequilibria and incompatible trace element ratios at Llaima are not source-derived features produced by combined mantle partial melting and/or slab-fluid addition. Mixing between a component with high ^{231}Pa and ^{238}U excesses and a component with small or no excesses appears to be the only process able to produce these linear arrays.

5.2. Origin of the component with high ^{231}Pa and ^{238}U excesses

The component with ^{231}Pa, ^{238}U, and ^{226}Ra excess required to anchor the high-disequilibrium ends of the Llaima mixing trends is characterized by high fluid-immobile incompatible element concentrations, high LILE/HFSE ratios, and unradiogenic Nd isotope ratios relative to N-MORB (Fig. 6). This component could be produced by melting of a mantle source less depleted than a typical N-MORB sources which would have been modified by slab fluids, as has generally inferred for SVZ magmas (Hickey et al., 1986; Lucassen et al., 2006).

To explore the conditions that can produce the ^{231}Pa, ^{238}U, and ^{226}Ra excesses in the high-disequilibrium mixing component, we have used two step models in which metasomatism of the mantle wedge by slab fluid is followed by dynamic partial melting. The activity ratios in the high-disequilibrium primary melt and the exact time spans between melting, crustal assimilation, and eruption are unknown. Consequently, the models presented only aim at reproducing the highest excesses measured in Llaima magmas and thus at constraining the limit of a range of possible solutions.

The mantle wedge source is assumed to be initially in secular equilibrium and to be characterized by a Th/U ratio of 3.3, which is compatible with an enriched MORB source (Sun and McDonough, 1989). The effect of metasomatism of this source was modeled by adding fluids in equilibrium with Chile rise MORBs that are subducting beneath the SVZ (Karsten et al., 1996). To calculate the composition of fluids, fluid/eclogite (subducted MORB) bulk partition coefficients from Klimm et al. (2008) and the compilation of Turner et al. (2003) were used. Fluids may also equilibrate with sediments overlying subducting MORBs. The fluid/eclogite bulk partition coefficients are unlikely to be drastically different for sediments and MORB compositions (Klimm et al., 2008). Metasomatism by fluids derived from U- and Th-rich sediments will lower the amount of fluid required in the models but will not affect the following observations.

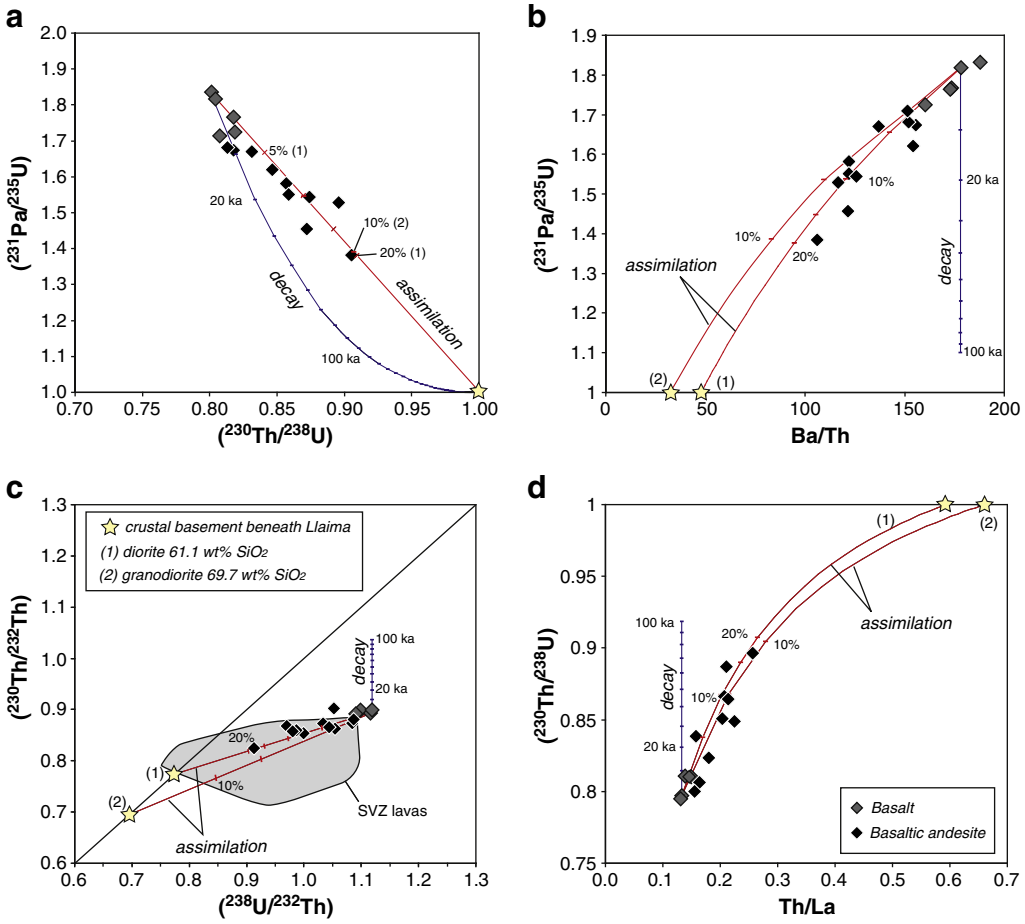

Fig. 4. U–Th–Pa activity and trace element ratios for Llaima historical magmas. Mixing curves show the effect of bulk assimilation of Tertiary diorite with 61.1 wt.% SiO_2 (1) and granodiorite with 69.7 wt.% SiO_2 (2) forming the basement beneath Llaima volcano [sample T-00-56 and T-00-59 from Lucassen et al. (2004); (Supplementary Table 3)]. These Tertiary rocks are assumed to be in secular equilibrium. (a) ($^{231}Pa/^{235}U$) vs. ($^{230}Th/^{238}U$). The curved trend shows the effect of radioactive decay. The diagonal linear trends are assimilation/mixing trends. (b) ($^{231}Pa/^{235}U$) vs. Ba/Th. (c) ($^{230}Th/^{232}Th$) vs. ($^{238}U/^{232}Th$) equiline diagram. The grey field shows U–Th activity ratios of SVZ magmas from (Jicha et al., 2007; Sigmarsson et al., 2002). (d) ($^{230}Th/^{238}U$) vs. Th/La. The AFC trends shown in Fig. 5b are very close from the assimilation trends on these diagrams and are not represented for clarity. Error bars are smaller than symbol size.

The metasomatised mantle source is assumed to start melting instantaneously after addition of slab-fluids, except for some of the models aiming at reproducing the ($^{226}Ra/^{230}Th$) ratios, for which the ^{226}Ra excesses produced by slab-fluid addition are allowed to decay back to equilibrium before melting (Fig. 7d). The formulation of Williams and Gill (1989) and partition coefficients from Blundy and Wood (2003) were used in our dynamic melting models. The extreme incompatibility of Pa causes ($^{231}Pa/^{235}U$) ratios to be controlled by the bulk partition coefficient of U (D_U), the residual porosity, and the partial melting rate of lherzolitic mantle. For a range of experimentally and theoretically estimated U mineral-melt partition coefficients (for a recent compilation see Stracke et al., 2006), the ^{231}Pa excess required in Llaima high-disequilibrium mixing component [($^{231}Pa/^{235}U$) ≈ 2] is attained for melting rates $<2\times10^{-4}$ kg/m^3/yr and residual porosities <0.6% (Fig 7a). These values overlap with estimates based, respectively, on crustal growth and petrological models (see Bourdon et al., 2003). Although the values of partition coefficients used to calculate the compositions of slab-derived fluids strongly affect the initial ($^{231}Pa/^{235}U$) and ($^{226}Ra/^{230}Th$) ratio of the mantle source, ^{231}Pa and ^{226}Ra in-growth during partial melting largely overcomes the initial disequilibria and ^{231}Pa and ^{226}Ra excesses in the melt show little dependence on the composition of the slab fluid (Fig. 7c and d). Addition of slab-fluid to the mantle wedge within a few thousand years (<8 kyr) of eruption would be required to produce ^{226}Ra excesses by slab-fluid addition as previously suggested for SVZ magmas (Sigmarsson et al., 2002). Fluid flux melting models taking into account continuous slab-fluid addition are however unable to reproduce the observed ^{231}Pa excess required to fit the Llaima data. In the case of Llaima, ^{226}Ra excesses may result from slab-fluid addition only in the event of late addition of fluids with Ra but no U.

The ($^{230}Th/^{238}U$) and ($^{230}Th/^{232}Th$) ratios increase with increasing D_U/D_{Th} during melting. The Llaima trend can be reproduced for values of D_U/D_{Th} between 0.7 and 0.8 (Fig. 7b). In addition, $D_U/D_{Th}<1$ during melting is necessary to sustain sufficient ^{238}U excesses at the low melting rates required to produce the observed ^{231}Pa excesses. During partial melting of lherzolitic mantle, U is more incompatible than Th only in clinopyroxene (Blundy and Wood, 2003; Wood et al., 1999) and D_U/D_{Th} in clinopyroxene decreases under increasingly oxidizing conditions (Lundstrom et al., 1994). Thus, the initial Pa, U, and Th disequilibria required in Llaima primary melt (i.e. the high U-series excesses component) suggest that clinopyroxene controls the U and Th budget during mantle melting and reflect the oxidized state of the metasomatised mantle source. The involvement of sediments via equilibration with slab fluids or as partial melts, as well as ageing of the source after addition of slab fluids would raise the ($^{230}Th/^{232}Th$) ratio of the metasomatised mantle source (Fig. 7b), requiring even lower D_U/D_{Th} ratios (<0.7) during melting.

The main outcome of these metasomatism and melting models is to demonstrate that melting processes are sufficient to produce the moderate ^{226}Ra excesses in Llaima magmas and that at the low melting rates required to account for the ^{231}Pa excesses, ($^{226}Ra/^{230}Th$)

Table 2
U–Th–Pa–Ra isotopic data for Volcán Llaima lavas.

Eruption	Sample	Th (ppm)	U (ppm)	^{226}Ra (fg/g)	2σm	^{231}Pa (fg/g)	2σm	$(^{238}U/^{232}Th)$	2σm	$(^{230}Th/^{232}Th)$	2σm	$(^{230}Th/^{238}U)$	2σm	$(^{234}U/^{238}U)$	2σm	$(^{231}Pa/^{235}U)$	2σm	$(^{226}Ra/^{230}Th)$ t=0	2σm
2008	508	1.37	0.49	169.8	1.0	276.9	1.8	1.085	0.001	0.875	0.004	0.807	0.004	1.001	0.001	1.712	0.006	1.269	0.013
1957	12c	1.38	0.47	173.5	1.1	250.9	1.8	1.034	0.001	0.875	0.003	0.846	0.003	1.003	0.003	1.620	0.006	1.298	0.011
1957	61	1.07	0.39	141.9	1.0	236.3	2.1	1.119	0.001	0.900	0.003	0.804	0.004	1.000	0.002	1.818	0.008	1.343	0.013
1780 SSW	33	1.44	0.47	175.8	0.9	247.5	2.0	0.999	0.001	0.855	0.002	0.857	0.003	1.000	0.003	1.582	0.006	1.309	0.010
1780 N	89	1.64	0.57	193.0	1.0	311.4	2.2	1.044	0.001	0.867	0.003	0.831	0.004	1.005	0.002	1.671	0.006	1.250	0.011
1780 SE	19	1.08	0.39	131.0	0.8	227.5	2.0	1.100	0.001	0.900	0.003	0.818	0.004	1.003	0.002	1.767	0.008	1.247	0.012
1780 S	208	0.97	0.36	117.2	0.6	214.5	1.7	1.117	0.001	0.895	0.003	0.802	0.004	1.003	0.002	1.833	0.007	1.254	0.011
1751	7	1.15	0.41	140.0	0.7	235.3	2.2	1.091	0.001	0.893	0.003	0.819	0.004	0.999	0.003	1.725	0.008	1.249	0.010
1903	95	2.44	0.73	277.5	1.9	334.9	2.8	0.914	0.001	0.827	0.003	0.905	0.004	0.999	0.003	1.384	0.006	1.248	0.012
1640	31	2.27	0.79	236.8	1.5	401.3	3.0	1.052	0.001	0.903	0.003	0.858	0.003	0.999	0.003	1.551	0.006	1.047	0.009
1640	385	2.52	0.82	256.4	1.3	393.3	3.4	0.988	0.001	0.861	0.003	0.871	0.004	1.002	0.002	1.457	0.006	1.085	0.010
1640	252	1.21	0.43	137.5	0.7	239.2	2.1	1.086	0.001	0.883	0.003	0.813	0.004	1.002	0.002	1.683	0.007	1.201	0.011
1903	85	1.61	0.52	184.8	0.8	264.5	1.9	0.980	0.001	0.857	0.003	0.874	0.004	0.997	0.002	1.545	0.006	1.225	0.011
1852	76	1.54	0.53	182.7	1.2	294.4	2.7	1.055	0.001	0.863	0.003	0.817	0.004	0.999	0.003	1.673	0.008	1.256	0.012
1852	74c	2.24	0.72	246.6	1.4	360.9	2.7	0.971	0.001	0.869	0.003	0.895	0.004	1.002	0.001	1.528	0.006	1.159	0.011
1852	23	1.14	0.41	135.4	0.8	238.2	3.0	1.091	0.001	0.892	0.003	0.818	0.004	0.999	0.002	1.764	0.011	1.222	0.012
	Standard				2 std. dev.		2 std. dev.				2 std. dev.		2 std. dev.		2 std. dev.		2 std. dev.		2 std. dev.
	BCR2	5.91	1.69	579.3	1.8	558.7	12.0	0.869	0.008	0.879	0.016	1.007	0.010	1.003	0.004	1.004	0.021	1.010	0.017
	W2	2.14	0.50	169.7	7.6	165.3	7.1	0.713	0.007	0.718	0.010	1.007	0.021	1.005	0.004	1.001	0.026	1.005	0.001

Activity ratios (denoted by parentheses) calculated using decay constants: $\lambda_{238} = 1.5513\times10^{-10}y^{-1}$, $\lambda_{234} = 2.8263\times10^{-6}y^{-1}$, $\lambda_{235} = 9.8485\times10^{-10}y^{-1}$, $\lambda_{232} = 4.9475\times10^{-11}y^{-1}$, $\lambda_{231} = 2.1158\times10^{-5}y^{-1}$, $\lambda_{230} = 9.1577\times10^{-6}y^{-1}$, $\lambda_{226} = 4.331\times10^{-4}y^{-1}$.

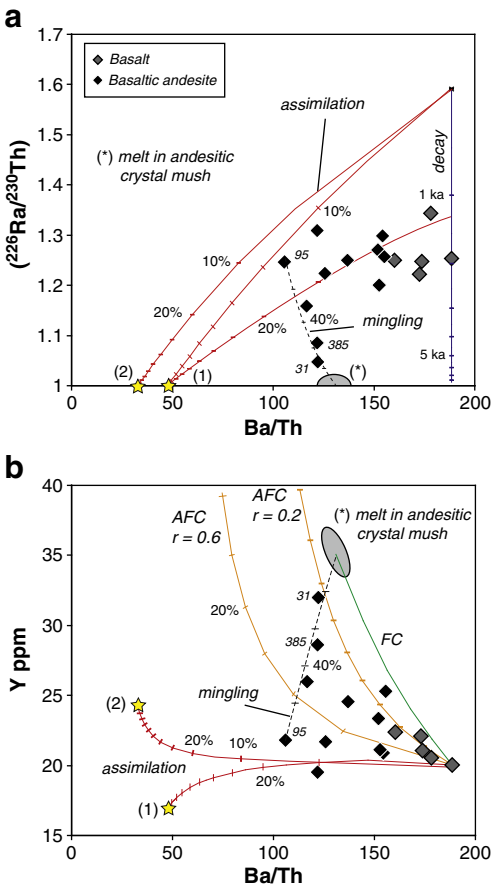

Fig. 5. (a) (^{226}Ra/^{230}Th) vs. Ba/Th diagram for Llaima lavas. The trend with time intervals shows the effect of radioactive decay. The curve labeled with percentages shows the effect of bulk assimilation of Tertiary basement diorite (1) and granodiorite (2) [sample T-00-56 and T-00-59 from Lucassen et al. (2004)]. The composition of the melts in the andesitic crystal mush is based on the composition of differentiated melt inclusions (~58 wt.% SiO_2) recording the low pressure crystallization trends of Llaima basaltic magmas (Bouvet de Maisonneuve, unpublished results). (b) Y vs. Ba/Th, crystallization trends correspond to the differentiation trends recorded by the melt inclusions as in (a). AFC trends are calculated using the formulation of DePaolo (1981) for two different ratios of assimilation rate to crystallization rate (r). Assimilation trends show the effect of assimilation of granitic rocks forming the basement beneath Llaima volcano as in Figs. 4 and 6. AFC trends are calculated using the diorite composition (T-00-59). Italic numbers next to some of the symbols are sample numbers. Samples 31 and 385 are from the same lava flow (1640S) and show petrographic evidence for mixing between a basaltic andesite magma and an andesitic crystal mush, suggesting that the AFC trends are in reality produced by a combination of magma mixing/mingling and assimilation of granitic rocks from the basement. If assimilation occurs on time scales much shorter than the half-life of ^{226}Ra (1.6 kyr), the AFC trends shown in (b) are very close to the assimilation trends in (a). The second mixing curve for the diorite (1) in (a) illustrates a scenario in which the mafic magmas had variable ^{226}Ra excesses prior to assimilation, possibly as a result of variable residence times in the crust. Alternatively, the range in (^{226}Ra/^{230}Th) ratios in lavas showing little evidence for mingling with andesitic crystal mush may indicate that assimilation occurred over time scales on the order of the half-life of ^{226}Ra. Error bars are smaller than symbol size.

disequilibria result from in-growth during melting. Consequently ^{226}Ra excesses, in the case of Llaima, do not unequivocally indicate slab-fluid addition to the mantle wedge shortly (<8 kyr) before eruption.

5.3. The secular equilibrium component

The (^{231}Pa/^{235}U) vs. (^{230}Th/^{238}U) array argues for a second mixing end-member component that is in, or near, secular equilibrium. Elliott et al. (1997) previously suggested the contribution of a component in U–Th secular equilibrium in Mariana arc magmas and interpreted it as an aged sediment melt. The inferred secular equilibrium component

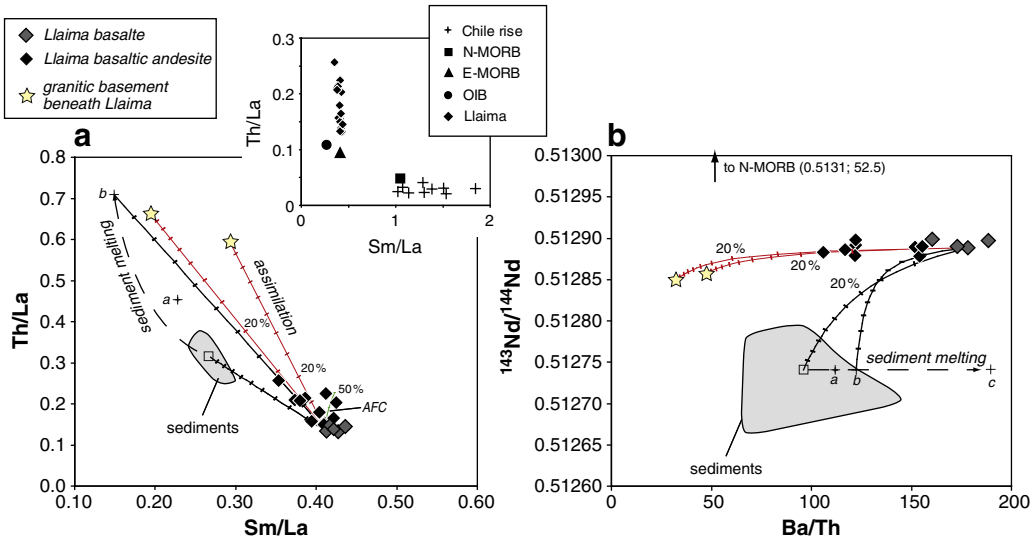

Fig. 6. Mixing models between Llaima's least differentiated magmas and bulk sediment, sediment melts, and Tertiary granitic rocks. (a) Th/La vs. Sm/La. (b) $^{143}Nd/^{144}Nd$ isotopes vs. Ba/Th. The grey sediment field shows the range of composition of sediments subducting beneath the SVZ (Lucassen et al., 2009). The average (open square) value was used for bulk assimilation models. Sediment melts were calculated for 10% batch melting using two sets of partition coefficients from (Johnson and Plank, 1999) (crosses a and b) and using melt/solid enrichment factors extracted from (Hermann and Rubatto, 2009) (cross c, these enrichment factors implicitly account for the residual sediment mineralogy, the type and degree of partial melting at the experimental conditions) (Supplementary Table 3). The assimilated granitic rocks are diorite and granodiorite as in Fig. 4 (data from Lucassen et al., 2009). Chile rise MORB data are from Karsten et al. (1996). Values for N-MORB, E-MORB and OIB are from Sun and McDonough (1989).

at Llaima is characterized by low Ba/Th (<100) and high Th/La (>0.25), Th/Nb (>1), and Th/Nd (>0.2). Such values are typical of continental margin sediment (Plank and Langmuir, 1998), but bulk assimilation of sediments that are being subducted beneath the SVZ (Lucassen et al., 2009) does not reproduce the observed trends (Fig. 6). Sediment partial melts, as argued for the Mariana magmas, are also unsatisfactory components due to their low $^{143}Nd/^{144}Nd$ and the high Ba/Th ratios produced by partial melting (Hermann and Rubatto, 2009; Johnson and Plank, 1999) (Fig. 6b) (Supplementary Table 3).

Turner et al. (2007) suggested that negative correlations between ($^{231}Pa/^{235}U$) and ($^{230}Th/^{238}U$) may be produced by mixing between deeper hydrous melts produced just above the slab with hotter and dryer melts produced at shallower depths by decompression melting. This model cannot explain the Llaima data because the component with low ^{231}Pa and ^{238}U excess should have a significantly higher Th/La ratio (>0.3) than N-MORB or E-MORB (0.048 and 0.095 respectively (Sun and McDonough, 1989)) as shown in Fig. 6a, and such ratios cannot reasonably be produced by melting of a mantle source.

These geochemical arguments plead against mantle melting, slab-fluid influx, and/or addition of sediments or sediment melts as explanations for the arrays observed at Llaima. The chemical and U-series variability defined by samples from single eruptions (Fig. 3) suggests that processes occurring in the upper crust, rather than in the mantle, control the U-series arrays. Assimilation of up to 20% of Tertiary diorite to granodiorite rocks of the Neogene subvolcanic basement beneath Llaima (Lucassen et al., 2004) (Fig. 1) reproduces the U-series and Nd isotope trends, as well as the trace element ratios (Figs. 4 and 6) (Supplementary Table 3), and provides a geologically realistic scenario. The assimilated granites represent the plutonic roots of earlier arc activity and they have Nd, Sr, and Pb isotopic ratios undistinguishable from Llaima lavas (Hickey et al., 1986; Lucassen et al., 2004). Consequently, assimilation is not identifiable on the basis of classical isotopic indicators of crustal input. The chemical heterogeneities in single lava flows indicate incomplete homogenization following assimilation. The maximum amounts of assimilation required by the models represent local maxima likely to mark the sites of digestion of small granitic fragments within the lava flows. The averaged percentages of assimilation for each flow are probably quite low (<5%).

Assimilation reproduces the isotope and incompatible trace element ratio arrays, incompatible trace element abundances require, however, combined assimilation and fractional crystallization (AFC) for some samples (Fig. 5b). The samples showing the strongest evidence for AFC come from the 1640S lava flow and these show petrographic evidence for mingling/mixing between a basaltic magma and an andesitic crystal mush (Dungan et al., in prep.). The AFC trends are therefore likely to represent a combination of late magma mixing/mingling and prior assimilation of granitic basement rocks. The variable AFC percentages and the range of assimilation/crystallization ratios required to fit the 1640S lava flow samples (Fig. 5b) most probably depict small scale heterogeneities in the proportion of mush-mixing and prior assimilation, as well as in the relative influence of these two processes. The low ($^{226}Ra/^{230}Th$) activity ratios in the samples showing the strongest evidence for magma mixing/mingling (Fig. 5a) indicates that the andesitic crystal mush was close to ($^{226}Ra/^{230}Th$) equilibrium, thereby suggesting that the residence times in the subvolcanic magmatic system of this mush were in excess of several kyr. The range in ($^{226}Ra/^{230}Th$) ratios in basaltic and basaltic andesite lavas showing little evidence for mingling with andesitic crystal mush suggest either that the mafic magmas had variable ^{226}Ra excesses prior to assimilation or that assimilation occurred over time scales on the order of the half-life of ^{226}Ra (1.6 kyr) (Fig. 5a). In both cases, this suggests that the residence times of the magmas in the crust were variable and long enough to result in a significant range of ^{226}Ra–^{230}Th disequilibria.

In summary, we propose that the remarkable linear correlations between ^{238}U and ^{231}Pa excesses and incompatible trace element ratios shown by Llaima historical magmas, are a consequence of assimilation of Tertiary granitic rocks forming the substratum of the volcano, i.e. the differentiated plutonic roots of the arc. Additional mixing/mingling between some of the "contaminated" basaltic andesite magmas and intermediate crystal mush several kyr old had limited impacts on ($^{230}Th/^{238}U$), ($^{231}Pa/^{235}U$), and ($^{230}Th/^{232}Th$) activity ratios and incompatible trace element ratios, but significantly affected the ($^{226}Ra/^{230}Th$) activity ratios and incompatible trace element abundances.

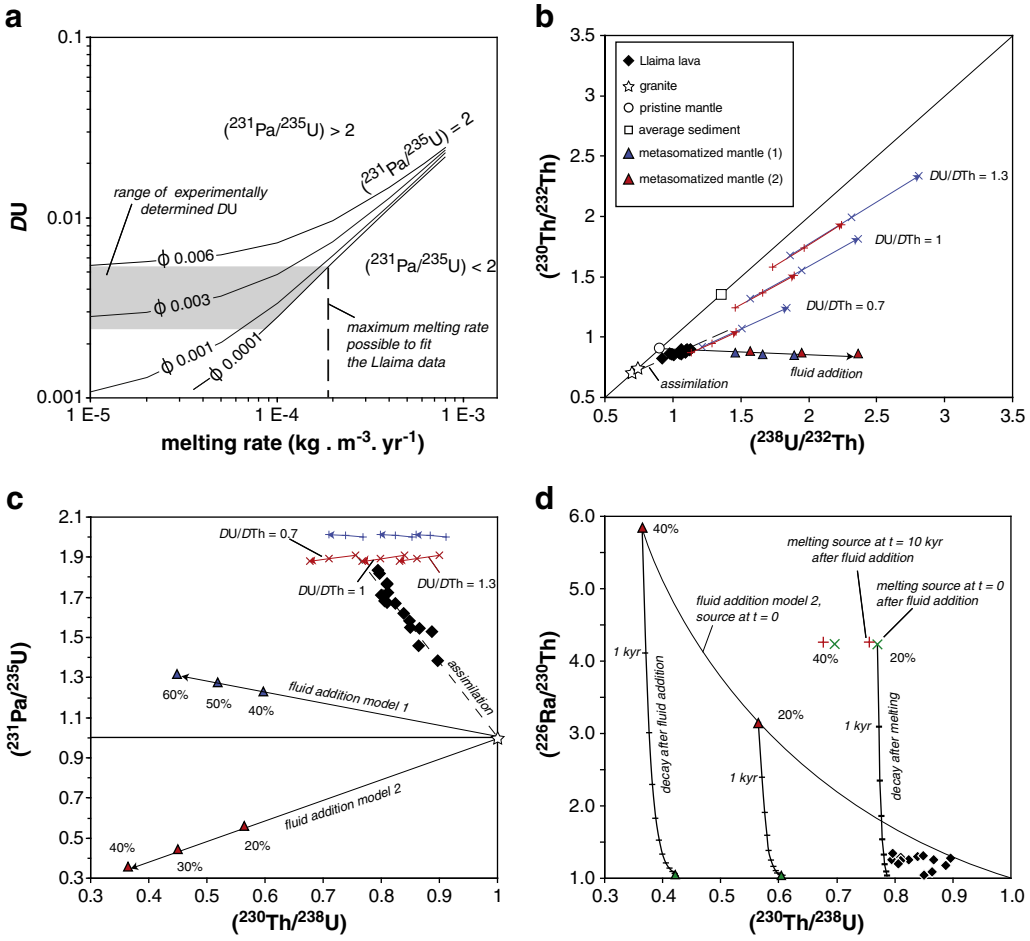

Fig. 7. Metasomatism, dynamic melting, and assimilation models. The source is assumed to be initially in secular equilibrium, to have a U/Th ratio of 3.3 typical of enriched MORB sources, and to be composed of 53% olivine + 27% orthopyroxene + 17% clinopyroxene + 3% spinel. Metasomatism by slab fluids was modeled assuming fluid equilibration with Chile rise MORBs (Karsten et al., 1996) and using the H_2O-rich fluid/eclogite bulk partition coefficients from Klimm et al. (2008) (model 1, blue triangles) and Turner et al. (2003) (model 2, red triangles). The metasomatised mantle source is assumed to start melting instantaneously after addition of slab-fluids, except for some of the models aiming at reproducing the (^{226}Ra/^{230}Th) ratios (in d). Dynamic melting calculations according to the formulation of Williams and Gill (1989) and partition coefficients from Blundy and Wood (2003). (a) (^{231}Pa/^{235}U) ratio as a function of D_U and melting rate. Black lines represent (^{231}Pa/^{235}U) = 2 for a range of source residual porosities (Φ). The metasomatised mantle source is here assumed to have (^{231}Pa/^{235}U) = 0.56 at the onset of melting, corresponding to 20% fluid addition in model 2. Melting rates up to 50% higher would produce (^{231}Pa/^{235}U) = 2 if the metasomatised mantle source had ^{231}Pa excesses as in model 2. (b) U–Th equiline diagram. The blue and red arrows show the effects of variable D_U/D_{Th} during melting of variably metasomatized mantle sources (blue and red arrows for sources calculated according to models 1 and 2 respectively). Dashed line shows the effect of assimilation of granodiorite forming the basement beneath Llaima volcano [sample T-00-56 and T-00-59 from Lucassen et al. (2004)]. (c) (^{231}Pa/^{235}U) vs. (^{230}Th/^{238}U) diagram showing the same features than in (b). Dynamic melting calculations for (^{226}Ra/^{230}Th) vs. (^{230}Th/^{238}U) (d) were done for two scenarios; (1) melting instantaneously after slab fluid addition, (2) melting 10 kyr after slab fluid addition, and for two amounts of slab fluid input calculated according to model 2. The curved trends in d show the effect of radioactive decay. Dynamic melting models in b, c and d were calculated for a melting rate of 1 E−4 kg/m^3/yr and residual porosities of 0.2%. Error bars are smaller than symbol size.

5.4. Implications for arc magmatism

Previous studies have shown that assimilation of crustal lithologies may exert significant leverage on U-series disequilibria. These conclusions have been based on correlations between U–Th disequilibria and Sr or Pb isotope ratios (Bourdon et al., 2000; Handley et al., 2008; Price et al., 2007). It has also been suggested that ^{230}Th excesses in continental arc magmas may result from assimilation of the lower crust (Bourdon et al., 2000; Garrison et al., 2006; Jicha et al., 2007). The Llaima dataset demonstrates that even in cases without obvious isotopic indications of crustal contamination, U-series systematics in conjunction with incompatible element ratios, can be affected by crustal assimilation if the contaminant is an earlier product of the arc activity with undistinguishable Nd, Sr and Pb isotopic ratios.

It could be argued that the Llaima case is applicable only to continental margin arc volcanoes, and that the effect of assimilation on U-series disequilibria is particularly significant owing to the low incompatible element contents of Llaima magmas and relatively high U and Th concentrations in the assimilated plutonic rocks. Nonetheless, assimilation (or mixing) of a component in secular equilibrium by magmas with U-series disequilibria typical of arc magmas can have significant effects even where contaminants are less enriched in U and Th; e.g. silicic magmas erupted at oceanic island arcs (Fig. 8). The life spans of most arc volcanoes (~10^5–10^6 yr) generally exceed the times necessary for U-series disequilibria to return to secular equilibrium. Ascending melts almost inevitably encounter and interact with products of crystallization of ancestral magmas at arc volcanoes (Dungan and Davidson, 2004; Reubi and Blundy, 2008; Reubi and Blundy, 2009). Assimilative recycling of the aged plutonic roots of arc volcanoes is likely to be widespread, but is difficult to monitor due to low Nd–Sr–Pb isotopic contrast. Linear arrays defined by activity ratios of nuclides with contrasting half-lives may be the most reliable indicators of assimilation of ancestral intrusive magmas.

Inclined U–Th isotope arrays similar to the one shown in Fig. 4c have been observed for several arcs and have been subject to multiple interpretations (Elliott et al., 1997; Turner et al., 2003). Predominant models involve addition of variable amount of slab-fluid and interpret the slope of these arrays as an indication that the time span between

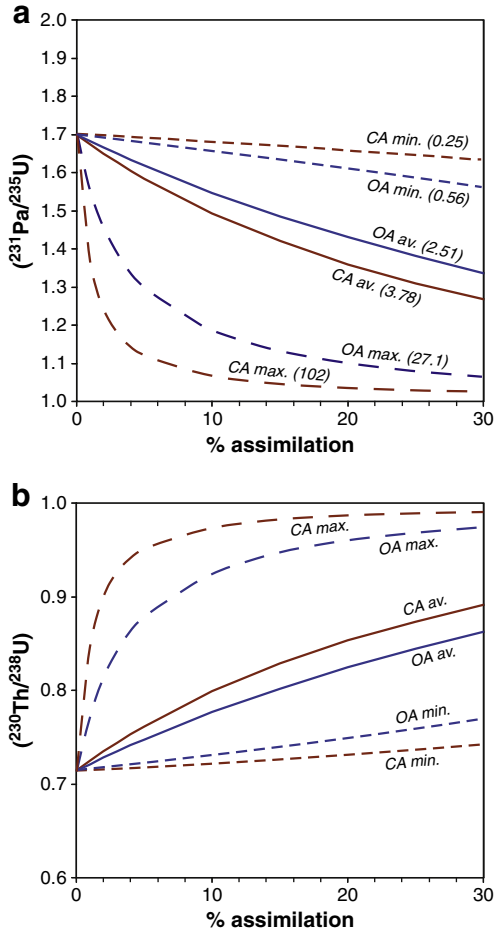

Fig. 8. Effect of assimilation of old arc magmas on U-series disequilibria. The curves represent the activity ratios of mafic magmas (<56 wt.% SiO_2) after assimilation of silicic magma (>65 wt.% SiO_2) erupted at the same volcanic arc. This shows possible extent of U-series disequilibria modification as a result of assimilation of silicic magmas left behind by the arc earlier activity (assimilation of plutonic roots) in a scenario similar to what is observed at Llaima. (a) ($^{231}Pa/^{235}U$) as a function of percentage of assimilation. (b) ($^{230}Th/^{238}U$) as a function of percentage of assimilation. The assimilating mafic magma is arbitrarily assumed to have an initial ($^{230}Th/^{238}U$) and ($^{231}Pa/^{235}U$) equal to 0.71 and 1.7 respectively. Such values are representative of the high ends of the ranges in ^{238}U and ^{231}Pa excesses in arc magmas (Turner et al., 2003). The contaminant is assumed to be in secular equilibrium. Curves are shown for continental arcs (CA) and oceanic arcs (OA). Values in brackets are ratios of U contents in assimilated silicic magmas over U contents in assimilating mafic magma ($U_{silicic}/U_{mafic}$). Minimum (min.) and maximum (max.) curves represent, respectively, the smallest and highest $U_{silicic}/U_{mafic}$ ratios in the data set. Average U contents in mafic magmas <56 wt.% SiO_2 and in silicic magmas >65 wt.% SiO_2 were used to calculate the average curves (av.). Data are from the GeoRoc database (http://georoc.mpch-mainz.gwdg.de/georoc/). Oceanic arc data are from the Marianna, Tonga, Kermadec and Izu-Bonin arcs. Continental arc data are from North, Central and South America.

fluid addition to the mantle wedge and eruption is typically between 20 and 150 kyr (Sigmarsson et al., 1990; Turner and Hawkesworth, 1997; Turner et al., 2001). In contrast, the positive correlation between Ba/Th and ^{226}Ra excesses observed in arc magmas has been interpreted by addition of slab fluids within a few hundred years before eruption (Turner et al., 2001). Assimilative recycling of differentiated plutonic rocks provides a simple and plausible alternative explanation for these apparent discrepancies in the time scales of slab fluid addition. The concomitant decreases in ($^{238}U/^{230}Th$) and ($^{226}Ra/^{230}Th$) with increasing SiO_2 observed in several island arcs have previously been acknowledged as a hint of the possible importance of assimilation of preexisting arc crust (Turner et al., 2001). The Llaima case establishes a well documented example of this process on the basis of multiple historic eruptions from one volcano and it demonstrates that assimilation can produce inclined U–Th isotope arrays and positively correlated ($^{238}U/^{230}Th$), ($^{226}Ra/^{230}Th$), and Ba/Th trends. Correlations between incompatible trace element ratios and U-series disequilibria, in this scenario, only hold information on the time scales of assimilation. As only the high-disequilibria ends of U-series arrays are significant in terms of mantle metasomatism and melting if assimilation prevails, the inference that globally correlated variations between Ba/Th, ^{226}Ra and ^{238}U excesses are a mantle source manifestation would become tenuous. This relaxes the necessity for time lags ~10^4–10^5 yr between U addition and melting, implying that U, Ra, and Ba could be added simultaneously to the mantle wedge. In the absence of correlations with other slab-fluid tracers, moderate ^{226}Ra excesses in the range of Llaima lavas cannot be considered as an irrevocable proof of recent (<8 kyr) slab-fluid addition, as dynamic melting can also generate these excesses.

6. Conclusions

Historical mafic magmas at Volcán Llaima have ranges in ^{238}U, ^{231}Pa, and ^{226}Ra excesses typical of arc magmas. Variations in U-series disequilibria observed for lavas from a single eruption cover up to 66% of the total measured range and are significant compared to the global ranges in arc magmas. Key features of the Llaima data are the strong linear correlations between ^{238}U and ^{231}Pa excesses and incompatible trace element ratios, indicating that the responsible processes operated on time scales significantly shorter than the half-life of ^{231}Pa (32 kyr). Such linear arrays cannot be produced by coupled slab-fluid influx and partial melting dynamics, or by addition of sediments or sediment melts to a mantle source. The preservation of U-series heterogeneities that are closely coupled with elemental ratios in single eruptions is difficult to reconcile with inheritance from mantle metasomatism or melting processes. A more plausible explanation is overprinting within the subvolcanic magmatic system. Bulk assimilation of 5–20% of basement granodioritic to dioritic rocks, respectively, beneath Llaima volcano, coupled with variable amounts of magma mixing/mingling in the subvolcanic magmatic system matches the U-series, Nd isotope, and incompatible trace element ratio arrays. Data from Llaima demonstrate that assimilation of the plutonic roots of the arc can impose intra-crustal U-series arrays on mantle signals with limited warning from traditional chemical indicators of crustal assimilation. Assimilation of differentiated magmas older than 350 kyr produces correlated U-series and incompatible trace element ratios arrays, which could be mistaken as indicators and chronometers of slab fluid addition, or tracers of sediment recycling. Cannibalization of ancestral magmas by ascending melts warrants careful consideration when considering chemical fluxes in subduction zones, but is difficult to monitor due to low Nd–Sr–Pb isotopic contrast. Linear arrays defined by U-series activity ratios of nuclides with contrasting half-lives could be the most robust indicators of assimilative recycling of plutonic roots of volcanoes by ascending magmas.

Supplementary materials related to this article can be found online at doi:10.1016/j.epsl.2010.12.018.

Acknowledgements

This work was supported by a Swiss NSF grant (20_125019) to M. Dungan. The manuscript was partly written while O. Reubi was supported by a Swiss NSF Ambizione fellowship. We thank Jose Antonio Naranjo, Alain Burgisser, Jason Jweda, Steve Goldstein, and Pablo Salas for participation in field work. We are grateful to A. Stracke for help with Nd isotope measurements, F. Oberli for his help to run the MC-ICPMS, L. Cooper for comments on an earlier version of the manuscript, and to C. Bouvet de Maisonneuve for participation in field work, sharing unpublished melt inclusion data and numerous discussions about the Llaima magmatic system. The manuscript was improved by reviews by S. Turner and an anonymous reviewer.

References

Allegre, C.J., Condomines, M., 1982. Basalt genesis and mantle structure studied through Th-iotopic geochemistry. Nature 299, 21–24.

Bezos, A., Escrig, S., Langmuir, C.H., Michael, P.J., Asimow, P.D., 2009. Origins of chemical diversity of back-arc basin basalts: a segment-scale study of the Eastern Lau Spreading Center. J. Geophys. Res. 114 (B06212), 1–25.

Blundy, J., Wood, B., 2003. Mineral-melt partitioning of uranium, thorium and their daughters, Uranium-Series Geochemistry. Rev. Mineral. Geochem. 52, 59–123.

Bourdon, B., Turner, S., Allegre, C., 1999. Melting dynamics beneath the Tonga-Kermadec Island are inferred from ^{231}Pa–^{235}U systematics. Science 286, 2491–2493.

Bourdon, B., Worner, G., Zindler, A., 2000. U-series evidence for crustal involvement and magma residence times in the petrogenesis of Parinacota volcano. Chile. Contrib. Mineral. Petrol. 139, 458–469.

Bourdon, B., Turner, S., Dosseto, A., 2003. Dehydration and partial melting in subduction zones: constraints from U-series disequilibria. J. Geophys. Res. 108 (B6), 1–19.

Davidson, J.P., Ferguson, K.M., Colucci, M.T., Dungan, M.A., 1988. The origin and evolution of magmas from the San-Pedro-Pellado volcanic complex, south Chile — multicomponent sources and open system evolution. Contrib. Mineral. Petrol. 100, 429–445.

Depaolo, D.J., 1981. Trace-element and isotopic effects of combined wallrock assimilation and fractional crystallization. Earth Planet. Sci. Lett. 53, 189–202.

Dosseto, A., Bourdon, B., Joron, J.L., Dupre, B., 2003. U–Th–Pa–Ra study of the Kamchatka arc: new constraints on the genesis of are lavas. Geochim. Cosmochim. Acta 67, 2857–2877.

Dungan, M.A., Davidson, J., 2004. Partial assimilative recycling of the mafic plutonic roots of arc volcanoes: an example from the Chilean Andes. Geology 32, 773–776.

Elliott, T., Plank, T., Zindler, A., White, W., Bourdon, B., 1997. Element transport from slab to volcanic front at the Mariana arc. J. Geophys. Res. 102, 14991–15019.

Garrison, J., Davidson, J., Reid, M., Turner, S., 2006. Source versus differentiation controls on U-series disequilibria: insights from cotopaxi volcano Ecuador. Earth Planet. Sci. Lett. 244, 548–565.

Gill, J.B., Williams, R.W., 1990. Th-isotope and U-series studies of subduction-related volcanic-rocks. Geochim. Cosmochim. Acta 54, 1427–1442.

Handley, H.K., Turner, S.P., Smith, I.E.M., Stewart, R.B., Cronin, S.J., 2008. Rapid timescales of differentiation and evidence for crustal contamination at intra-oceanic arcs: geochemical and U–Th–Ra–Sr–Nd isotopic constraints from Lopevi Volcano, Vanuatu SW Pacific. Earth Planet. Sci. Lett. 273, 184–194.

Hermann, J., Rubatto, D., 2009. Accessory phase control on the trace element signature of sediment melts in subduction zones. Chem. Geol. 265, 512–526.

Hickey, R.L., Frey, F.A., Gerlach, D.C., Lopezescobar, L., 1986. Multiple sources for basaltic arc rocks from the Southen Volcanic Zone of the Andes (34 degrees S–41 degrees S). Trace element and isotopic evdience fo contributions from subducted oceanic crust, mantle and continental crust. J. Geophys. Res. 91, 5963–5983.

Hickey-Vargas, R., Sun, M.R., Lopez-Escobar, L., Moreno-Roa, H., Reagan, M.K., Morris, J.D., Ryan, J.G., 2002. Multiple subduction components in the mantle wedge: evidence from eruptive centers in the Central Southern volcanic zone, Chile. Geology 30, 199–202.

Hildreth, W., Moorbath, S., 1988. Crustal Contributions to Arc Magmatism in the Andes of Central Chile. Contrib. Mineral. Petrol. 98, 455–489.

Huang, F., Lundstrom, C.C., 2007. ^{231}Pa excesses in arc volcanic rocks: constraint on melting rates at convergent margins. Geology 35, 1007–1010.

Huang, F., Gao, L., Lundstrom, C.C., 2008. The effect of assimilation, fractional crystallization, and ageing on U-series disequilibria in subduction zone lavas. Geochim. Cosmochim. Acta 72, 4136–4145.

Jicha, B.R., Singer, B.S., Beard, B.L., Johnson, C.M., Roa, H.M., Naranjo, J.A., 2007. Rapid magma ascent and generation of Th-230 excesses in the lower crust at Puyehue-Cordon Caulle, Southern Volcanic Zone Chile. Earth Planet. Sci. Lett. 255, 229–242.

Johnson, M.C., Plank, T., 1999. Dehydration and melting experiments constrain the fate of subducted sediments. Geochem. Geophys. Geosys. 1, 1–26.

Karsten, J.L., Klein, E.M., Sherman, S.B., 1996. Subduction zone geochemical characteristics in ocean ridge basalts from the southern Chile Ridge: implications of modern ridge subduction systems for the Archean. Lithos 37, 143–161.

Klimm, K., Blundy, J.D., Green, T.H., 2008. Trace element partitioning and accessory phase saturation during H_2O-saturated melting of basalt with implications for subduction zone chemical fluxes. J. Petrol. 49, 523–553.

Koornneef, J.M., Stracke, A., Aciego, S., Reubi, O., Bourdon, B., 2010. A new method for U–Th–Pa–Ra separation and accurate measurement of ^{234}U–^{230}Th–^{231}Pa–^{226}Ra disequilibria in volcanic rocks by MC-ICPMS. Chem. Geol. 277, 30–41.

Lucassen, F., Trumbull, R., Franz, G., Creixell, C., Vasquez, P., Romer, R.L., Figueroa, O., 2004. Distinguishing crustal recycling and juvenile additions at active continental margins: the Paleozoic to recent compositional evolution of the Chilean Pacific margin (36–41°S). J. South Amer. Earth Sci. 17, 103–119.

Lucassen, F., Kramer, W., Bartsch, V., Wilke, H.G., Franz, G., Romer, R.L., Dulski, P., 2006. Nd, Pb, and Sr isotope composition of juvenile magmatism in the Mesozoic large magmatic province of northern Chile (18–27°S): indications for a uniform subarc mantle. Contrib. Mineral. Petrol. 152, 571–589.

Lucassen, F., Wiedicke, M., Franz, G., 2009. Complete recycling of a magmatic arc: evidence from chemical and isotopic composition of Quaternary trench sediments in Chile (36–40°S). Int. J. Earth Sci. 3, 687–701.

Lundstrom, C., Shaw, H., Ryerson, F., Phinney, D., Gill, J., Williams, Q., 1994. Compositional controls on the partitioning of U, Th, Ba, Pb, Sr and Zr between clinopyroxene and haplobasaltic melts — implications for Uranium series disequilibria in basalts. Earth Planet. Sci. Lett. 128, 407–423.

McDermott, F., Hawkesworth, C., 1991. Th, Pb, and Sr isotope variations in Young Island-Arc volcanics and oceanic sediments. Earth Planet. Sci. Lett. 104, 1–15.

Naranjo, J.A., Moreno, H., 2005. Geología del Volcán Llaima, región de la Araucanía. Carta geológica de Chile, serie geología básica, 88. Servicio Nacional de Geologia y Mineria, Santiago. 33pp.

Pfeifer, H.R., Lavanchy, J.C., Serneels, V., 1991. Bulk chemical and industrial materials by X-ray fluorescence, recent developments and application to material rich in iron oxides. J. Trace Micropro. Tech. 9, 127–147.

Pickett, D.A., Murrell, M.T., 1997. Observations of ^{231}Pa–^{235}U disequilibrium in volcanic rocks. Earth Planet. Sci. Lett. 148, 259–271.

Pin, C., Zalduegui, J.F.S., 1997. Sequential separation of light rare-earth elements, thorium and uranium by miniaturized extraction chromatography: application to isotopic analyses of silicate rocks. Analyt. Chim. Acta 339, 79–89.

Plank, T., Langmuir, C.H., 1998. The chemical composition of subducting sediment and its consequences for the crust and mantle. Chem. Geol. 145, 325–394.

Price, R.C., George, R., Gamble, J.A., Turner, S., Smith, I.E.M., Cook, C., Hobden, B., Dosseto, A., 2007. U–Th–Ra fractionation during crustal-level andesite formation at Ruapehu volcano, New Zealand. Chem. Geol. 244, 437–451.

Reubi, O., Blundy, J., 2008. Assimilation of plutonic roots, formation of high-K exotic melt inclusions and genesis of andesitic magmas at Volcán de Colima, Mexico. J. Petrol. 49, 2221–2243.

Reubi, O., Blundy, J., 2009. A dearth of intermediate melts at subduction zone volcanoes and the petrogenesis of arc andesites. Nature 461, 1269–1273.

Sigmarsson, O., Condomines, M., Morris, J.D., Harmon, R.S., 1990. Uranium and Be-10 enrichments by fluids in Andean arc magmas. Nature 346, 163–165.

Sigmarsson, O., Chmeleff, J., Morris, J., Lopez-Escobar, L., 2002. Origin of ^{226}Ra–^{230}Th disequilibria in arc lavas from southern Chile and implications for magma transfer time. Earth Planet. Sci. Lett. 196, 189–196.

Stracke, A., Bourdon, B., McKenzie, D., 2006. Melt extraction in the Earth's mantle: Constraints from U–Th–Pa–Ra studies in oceanic basalts. Earth Planet. Sci. Lett. 244, 97–112.

Sun, S.S., McDonough, W.F., 1989. Chemical and isotopic systematics of oceanic basalts: implications for mantle composition and processes. In: Saunders, A.D., Norry, M.J. (Eds.), Magmatism in the Ocean Basins, vol. 42. Geological Society of London Special Publication, pp. 313–345.

Tanaka, T., Togashi, S., Kamioka, H., Amakawa, H., Kagami, H., Hamamoto, T., Yuhara, M., Orihashi, Y., Yoneda, S., Shimizu, H., Kunimaru, T., Takahashi, K., Yanagi, T., Nakano, T., Fujimaki, H., Shinjo, R., Asahara, Y., Tanimizu, M., Dragusanu, C., 2000. JNdi-1: a neodymium isotopic reference in consistency with La Jolla neodymium. Chem. Geol. 168, 279–281.

Tassara, A., Swain, C., Hackney, R., Kirby, J., 2007. Elastic thickness structure of South America estimated using wavelets and satellite-derived gravity data. Earth Planet. Sci. Lett. 253, 17–36.

Thomas, R.B., Hirschmann, M.M., Cheng, H., Reagan, M.K., Edwards, R.L., 2002. (Pa-231/U-235)–(Th-230/U-238) of young mafic volcanic rocks from Nicaragua and Costa Rica and the influence of flux melting on U-series systematics of arc lavas. Geochim. Cosmochim. Acta 66, 4287–4309.

Tormey, D.R., Hickey-Vargas, R., Frey, F.A., Lopezescobar, L., 1991. Recent lavas from the Andean front (33 to 42 S): interpretations of along-arc compositional variations. In: Harmon, R.S., Rapela, C.W. (Eds.), Andean Magmatism and Its Tectonic Setting: Geol. Soc. Amer. Spec. paper, Volume 265, pp. 57–77.

Turner, S., Hawkesworth, C., 1997. Constraints on flux rates and mantle dynamics beneath island arcs from Tonga-Kermadec lava geochemistry. Nature 389, 568–573.

Turner, S., Bourdon, B., Hawkesworth, C., Evans, P., 2000. ^{226}Ra–^{230}Th evidence for multiple dehydration events, rapid melt ascent and the time scales of differentiation beneath the Tonga-Kermadec island arc. Earth Planet. Sci. Lett. 179, 581–593.

Turner, S., Evans, P., Hawkesworth, C., 2001. Ultrafast source-to-surface movement of melt at island arcs from ^{226}Ra–^{230}Th systematics. Science 292, 1363–1366.

Turner, S., Bourdon, B., Gill, J., 2003. Insights into magma genesis at convergent margins from U-series isotopes Uranium-Series Geochemistry. Rev. Mineral. Geochem. 52, 255–315.

Turner, S., Regelous, M., Hawkesworth, C., Rostami, K., 2006. Partial melting processes above subducting plates: constraints from ^{231}Pa–^{235}U disequilibria. Geochim. Cosmochim. Acta 70, 480–503.

Turner, S., Sims, K.W.W., Reagan, M., Cook, C., 2007. A ^{210}Pb–^{226}Ra–^{230}Th–^{238}U study of Klyuchevskoy and Bezymianny volcanoes Kamchatka. Geochim. Cosmochim. Acta 71, 4771–4785.

Williams, R.W., Gill, J.B., 1989. Effects of partial melting on the uranium decay series. Geochim. Cosmochim. Acta 53, 1607–1619.

Wood, B.J., Blundy, J.D., Robinson, J.A.C., 1999. The role of clinopyroxene in generating U-series disequilibrium during mantle melting. Geochim. Cosmochim. Acta 63, 1613–1620.

Yokoyama, T., Kuritani, T., Kobayashi, K., Nakamura, E., 2006. Geochemical evolution of a shallow magma plumbing system during the last 500 years, Miyakejima volcano, Japan: constraints from ^{238}U–^{230}Th–^{226}Ra systematics. Geochim. Cosmochim. Acta 70, 2885–2901.